Supporting Information

Platinum Monolayer Dispersed on MXenes for Electrocatalyzed Hydrogen Evolution: A First-Principles Study

Mingqi He,[a] Yanan Zhou,[b] Qiquan Luo,*,[c] and Jinlong Yang*,[a]

[a]Department of Chemical Physics, Key Laboratory of Precision and Intelligent Chemistry, Hefei National Research Center for Physical Sciences at the Microscale, University of Science and Technology of China, Hefei, Anhui 230026, China

[b]School of Material Science and Chemical Engineering, Institute of Mass Spectrometry, Ningbo University, Fenghua Road 818, Ningbo 315211, China

[c]Institutes of Physical Science and Information Technology, Anhui University, Hefei, Anhui 230601, China

**Email: qluo@ahu.edu.cn; jlyang@ustc.edu.cn

Table of contents:

Computational Details

All spin-polarized density functional theory (DFT) calculations were performed using the Vienna *ab initio* Simulation Package (VASP) code.[1, 2] The projector augmented wave (PAW) method was used to describ the influence of ionic cores on the valence electrons. Electron exchange and correlation interactions were calculated with the Perdew-Burke-Ernzerhof functional in the general gradient approximation (GGA-PBE) and the plane-wave cutoff energy of 500 eV was adopted.[3, 4] The Grimme's D3 correction method was applied to account for the van der Waals (vdW) dispersion interaction.[5] Convergence criteria for geometric relaxation were defined as the forces on each atom being less than 0.02 eV/Å, and energy convergence criteria for all self-consistent field calculations were set as 10^{-5} eV. The k-point meshes of (9×9×1) and (12×12×1) were used for sample the Brillouin zone in geometric optimizations and electronic structure calculations, respectively.[6] A vacuum slab of 20 Å was employed to separate two periodic surfaces in the *z*-direction. *Ab initio* molecular dynamics (AIMD) simulations were performed to evaluate the thermal stability of the structure, using the NVT ensemble controlled by the Nosé-Hoover method over 10 ps with a time step of 1 fs.[7, 8] The Bader charge analysis was used to obtain the charge transfer.[9] The crystal orbital Hamilton population (COHP) analysis was adopted to analyze the bonding/antibonding population between Pt atoms using the LOBSTER package.[10, 11] The energy barrier were computed using the climbing image nudged elastic band (CI-NEB) method [12], assuming that each protonation step transfers one integer electron, with the Eigen cations model representing the source of protons.

The adsorption energy of *H and the Gibbs free energy change for *H are calculated under the standard conditions (T = 298.15 K, U = 0, pH = 0):

$$\Delta G_{*\mathrm{H}} = \Delta E_{*\mathrm{H}} + \Delta ZPE - \mathrm{T}\Delta S \quad (1)$$

$$\Delta E_{*\mathrm{H}} = E_{*\mathrm{H}} - E_{*} - \frac{1}{2}E_{\mathrm{H_2}} \quad (2)$$

where $\Delta E_{*\mathrm{H}}$ is the energy difference based on DFT calculations, ΔZPE is the zero-point energy (ZPE) correction, T is the temperature and set as 298.15 K, and ΔS is the entropy change. [13] In this work, $\Delta ZPE - T\Delta S$ is applied 0.24 eV based on the literature.[14, 15] The adsorption energy of H on the 3×3 supercell, where ΔG(*H) is -0.04 eV, is closer to the value for the 2×2 supercell (-0.06 eV).

The average adsorption energy ($E_{\mathrm{ads(avg)}}$) (also called the integral adsorption energy) and the stepwise adsorption energy ($E_{\mathrm{ads(step)}}$) of hydrogen are calculated as follows:

$$E_{\mathrm{ads(avg)}} = (E_{*+\mathrm{nH}} - E_{*} - \frac{n}{2}E_{\mathrm{H_2}})/n \quad (3)$$

$$E_{\mathrm{ads(step)}} = E_{*+\mathrm{nH}} - E_{*+(\mathrm{n-1})\mathrm{H}} - \frac{1}{2}E_{\mathrm{H_2}} \quad (4)$$

where n is the number of H atoms in the calculation.

Surface Pourbaix diagram

The surface Pourbaix diagram was computed as a function of potential and pH using the computational hydrogen electrode (CHE) method proposed by Nørskov et al.[16, 17] The different surface terminations are considered to be in equilibrium with water, proton, and electrons, through the following steps:

$$slab + xH_2O \rightarrow slab - O_xH_y + (2x - y)(H^+ + e^-) \quad (5)$$

$$slab + z(H^+ + e^-) \rightarrow slab - H_z \quad (6)$$

where slab-O_xH_y denotes the oxidized surface, with x and y representing the number of O and H atoms adsorbed on the bare surface, respectively. And slab-H_z refers to the reduced surface, where z denotes the number of H atoms. The free energies of different surface states in the surface Pourbaix diagram can be calculated as follows:

$$\Delta G_1(U, pH) = G(slab - O_xH_y) + (2x - y)[1/2G(H_2) - eU_{SHE} - k_BT\ln 10 \times \mathrm{pH}] - G(slab) - xG(H_2O) \quad (7)$$

$$\Delta G_2(U, pH) = G(slab - H_z) - z[1/2G(H_2) - eU_{SHE} - k_BT\ln 10 \times \mathrm{pH}] - G(slab) \quad (8)$$

where G(slab-O_xH_y), G(slab-H_z), G(slab), $G(H_2)$, and $G(H_2O)$ represent the total free energies of the oxidized surface, the reduced surface, the clean surface, a hydrogen molecule, and a water molecule, respectively. U_{SHE} denotes the potential referenced to the standard hydrogen electrode (SHE), k_B is the Boltzmann constant and T is the temperature (at 298.15 K). For each given potential and pH, the surface termination with the lowest free energy will be depicted on the surface Pourbaix diagram.

The surface Pourbaix diagrams of pure Pt and Mo_2TiC_2 catalyst for stability analysis have been reported previously. For Pt(111), it is shown that at potential below 0.78V, the pure Pt surface without adsorbates is the most stable.[16, 18] For Mo_2TiC_2, it might fully terminated by O* under standard conditions, $|\Delta G(*H)| \geq 0.26$ at different H coverage.[19]

Interfacial formation energy

To compare the stability of possible adsorption sites for Pt monolayer on Mo_2TiC_2, the formation energy of the interface is defined by:

$$E_{\mathrm{form}} = E_{\mathrm{slab}} - E_{\mathrm{Pt\text{-}monolayer}} - E_{\mathrm{sub}} \quad (9)$$

where E_{slab} is the total energy of Pt_{ML}/Mo_2TiC_2, E_{sub} is the total energy of the Mo_2TiC_2 substrate and $E_{\mathrm{Pt\text{-}monolayer}}$ is the total energy of the Pt monolayer. The more negative E_{form} is, the more stable the Pt_{ML}/Mo_2TiC_2 interface. The calculated formation energies are given in Table S1.

Dissolution potential

The dissolution potential (U_{diss})[20] was used to estimate the electrochemical stability of Pt_{ML}/Mo_2TiC_2, calculated by the following equation:

$$ne(U_{diss} - U^{\circ}_{diss}) = E_{Pt,bulk} - \frac{E_{ML} - E_{noML}}{N_{surf}} \quad (10)$$

where $U^{\circ}_{\mathrm{diss}}$ and n are the standard dissolution potential of bulk metal (Pt) and the number of electrons required to oxidize the metal, respectively, obtained from the NIST database. $E_{\mathrm{Pt,bulk}}$ equals to the total energy per atom for bulk Pt. E_{ML} and E_{noML} are the total energy of Mo_2TiC_2 with and without the Pt monolayer, respectively. N_{surf} is the number of the surface monolayer Pt atoms per supercell. The calculated dissolution potential for Pt_{ML}/Mo_2TiC_2 is 1.62 V, which is higher than that of Pt bulk (1.18 V, where 1.18 V is the standard dissolution potential of bulk metal), indicating the stability of the proposed Pt monolayer structure under operating conditions. Additionally, the calculated dissolution potential for Pt_1/Mo_2TiC_2 is 1.29 V, which is a single atom Pt anchored on Mo_2TiC_2. We have calculated the ΔG(*H) of Pt_1/Mo_2TiC_2 (0.03 eV), which is also close to 0 eV, indicating good HER activity. However, according to the dissolution potential calculation results,

Pt_{ML}/Mo_2TiC_2 is more stable.

Constant potential method (CPM)

The double-reference method was employed to simulate the electrode and solution interfaces in electrochemistry and to evaluate the influence of solvation and the applied potential on the reaction.[21-27] The solvent effect was considered by using the implicit solvent model as implemented in VASPsol, with the dielectric constant of 78.4 for water.[28] The electric potential of the slab reference to the standard hydrogen electrode (SHE) is calculated as follows:

$$U_q(V/SHE) = -4.6 - \Phi_q(f)/eV \qquad (11)$$

where $\Phi_q(f)$ represents the work function of the charged slab in aqueous solution, and 4.6 V is the work function of the H_2/H^+ couple at standard conditions. The total energy of the charged system is corrected for the interaction with the background charge as well as for the difference in the number of electrons in the system by:

$$E_{corr} = \int_0^q \langle \overline{V_{tot}} \rangle dQ + qU_q \qquad (12)$$

For each structure, calculations are performed at charges of -1.5e to +1.5e with steps of +0.5e. The total free energy at the 7 charge values is fitted to a quadratic function to provide the free energy as a continuous function of potential. This quadratic form aligns with a capacitor formed by the charged-slab/background-charge system, described as:

$$E(U) = -\frac{1}{2}C(U - U_0)^2 + E_0 \qquad (13)$$

where U_0 refers to the potential of zero charge (PZC), E_0 is the energy at the PZC, and C is the capacitance of the surface. Utilizing the fitted quadratic functions for both the bare slab and slabs with adsorbates, the binding energies and reaction energetics can be determined as a function of electric potential.

Indeed, altering the pH value results in a change in the electric potential on the SHE scale at a fixed potential on the reversible hydrogen electrode (RHE)scale, according to the relation:

$$U_{RHE} = U_{SHE} + k_B T \ln(10) \times pH/e \qquad (14)$$

Based on the relationship between the electric potential U_{RHE} and U_{SHE}, a change in pH value by ΔpH would shift the U_{SHE} by $k_B T \ln 10 \times \Delta pH$.

HER polarization curve

The theoretical exchange current (i_0) based on the assumption is proposed by Nørskov et al.,[14] as following at pH = 0:

$$i_0 = -ek_0 \frac{1}{1 + \exp(|\Delta G(*H)|/k_B T)} \qquad (15)$$

where k_0 is the rate constant.

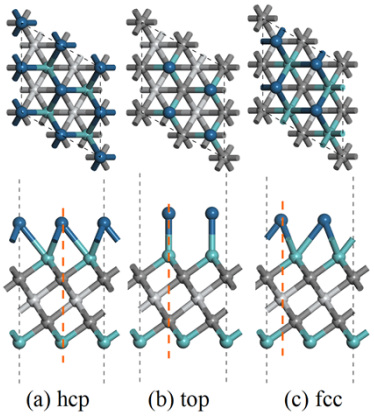

Fig. S1. Different possible positions of Pt monolayer on Mo_2TiC_2: (a) hexagonal close-packed (hcp), (b) top, and (c) face center cubic (fcc). Green, blue, dark gray, and light gray spheres denote Mo, Pt, C, and Ti, respectively.

Notes: Comparison between the possible adsorption site for Pt monolayer on Mo_2TiC_2, Pt on hcp sites (a) has the lowest energy and is also the structure in the maintext **Fig. 1a**.

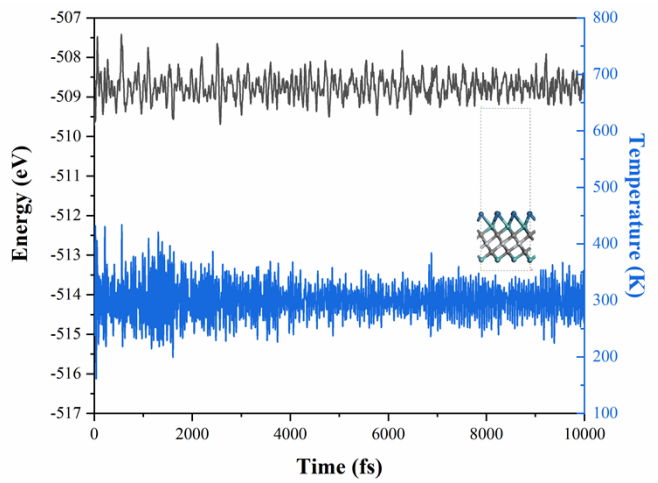

Fig. S2. Variations of the total energy and temperature towards time for AIMD simulations of Pt_{ML}/Mo_2TiC_2 for 10 ps at 300K. Insets are the side view of a snapshot of the atomic configuration at 10 ps.

Notes: There is an energy difference between the static DFT calculations and AIMD simulations, which could be mainly attributed to lattice vibrations. Specifically, using the Debye model, we roughly estimated that lattice vibrations at 300K caused a 4.19 eV change. ($U \approx kT \cdot 3N\left(\frac{T}{\Theta_D}\right)^3$,where k is the Boltzmann constant, 8.617×10^{-5} eV/K; T is the AIMD simulations temperature of 300K; N is the number of atoms, with the Pt_{ML}/Mo_2TiC_2 system containing 54 atoms; and Θ_D is the Debye temperature, estimated here as 300 K by referring to the Debye temperature of common solids.).

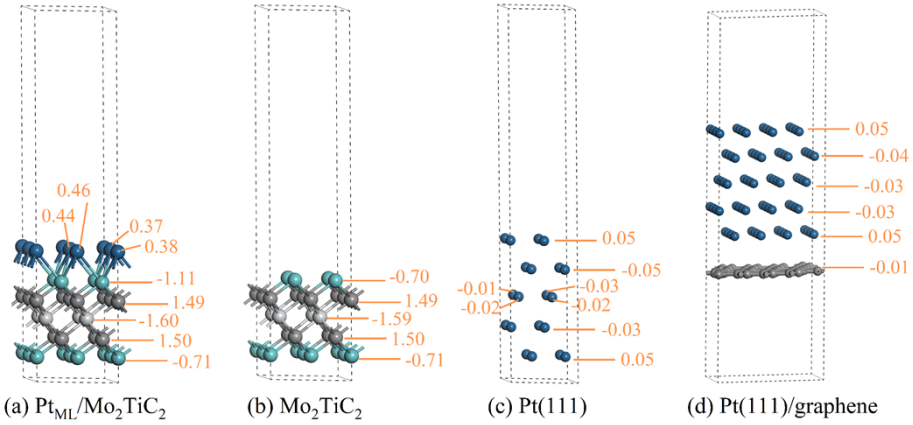

Fig. S3. Bader charge of (a) Pt_{ML}/Mo_2TiC_2, (b) Mo_2TiC_2, (c) Pt(111), and (d) Pt(111)/graphene.

Notes: For simulation Pt/C, a (4×4) supercell Pt(111)/graphene with a total of 80 Pt atoms and 42 C atoms in graphene layer was used, measuring whether there is charge transfer between the metal (Pt(111)) and the carbon substrate.

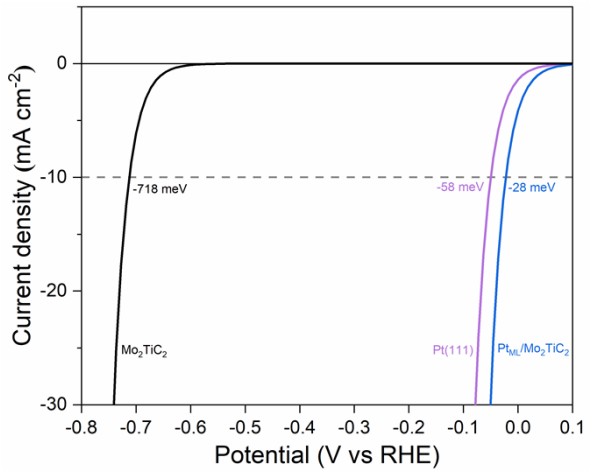

Fig. S4. Simulated HER polarization curves of the Pt_{ML}/Mo_2TiC_2, Mo_2TiC_2, and Pt(111) surface.

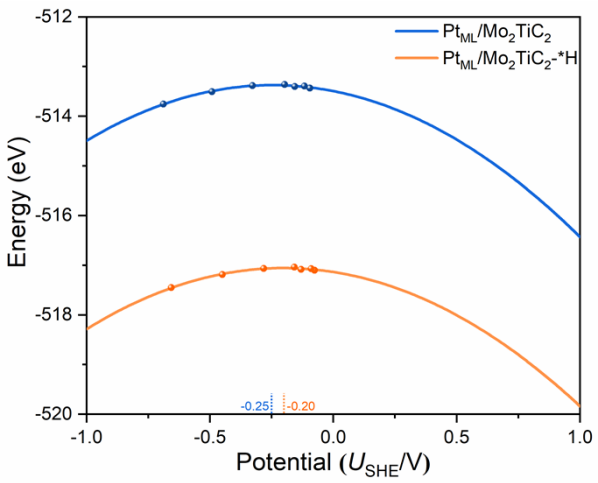

Fig. S5. The total energies of bare Pt_{ML}/Mo_2TiC_2 and adsorption *H on Pt_{ML}/Mo_2TiC_2 as a function of applied potential U_{SHE}.

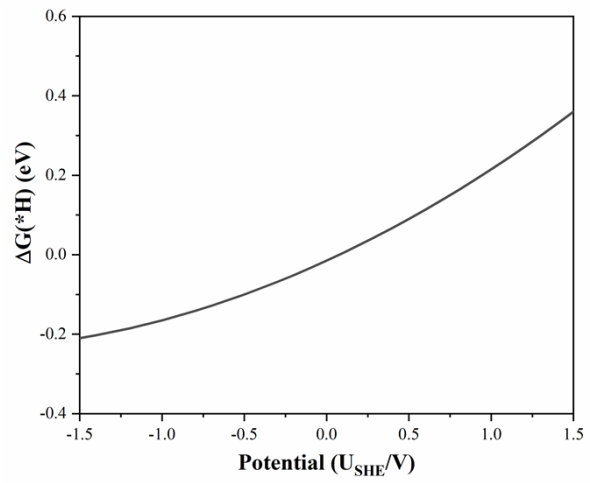

Fig. S6. Adsorption energy of *H as a function of U_{SHE} on Pt_{ML}/Mo_2TiC_2.

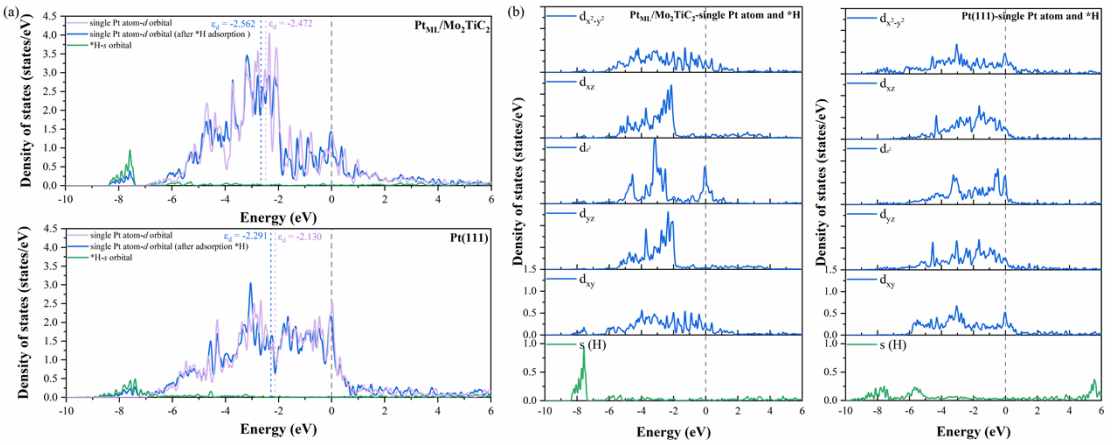

Fig. S7. (a) PDOS of single Pt atom before and after adsorption *H on Pt_{ML}/Mo_2TiC_2 and Pt(111). **(b)** PDOS of *d* orbital of single Pt atom and *s* orbital of adsorption *H on Pt_{ML}/Mo_2TiC_2 and Pt(111). The Fermi level is assigned at 0 eV.

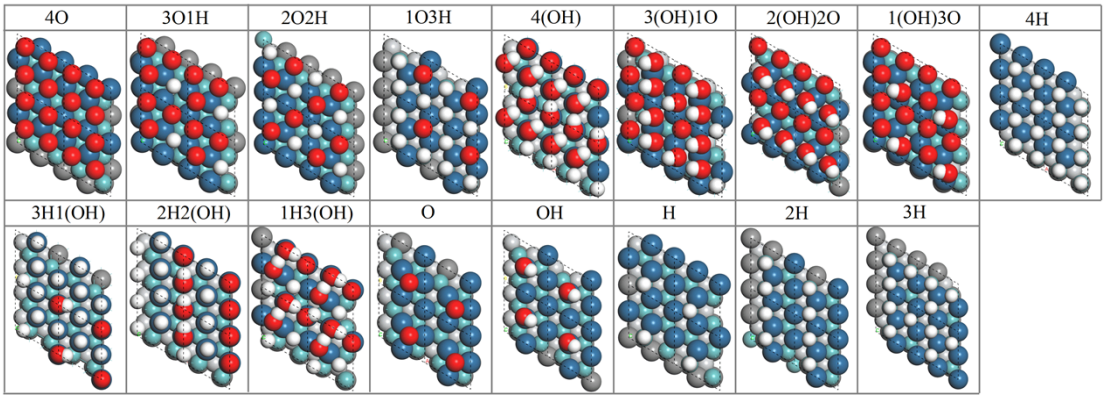

Fig. S8. Top view of atomic adsorption configurations corresponding to different surface coverages in the surface Pourbaix diagram of Pt_{ML}/Mo_2TiC_2.

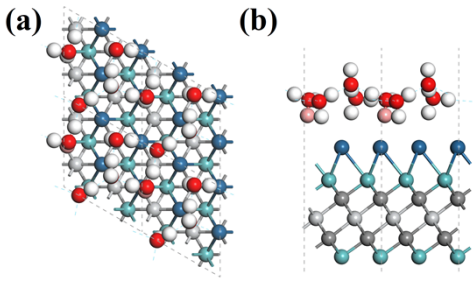

Fig. S9. (a) Top view and (b) side view of $H_3O^+(H_2O)_3$ or $H_9O_4^+$ ontop of Pt_{ML}/Mo_2TiC_2.

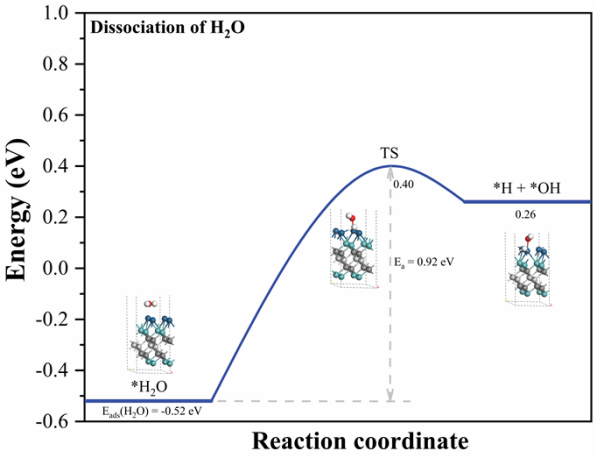

Fig. S10. Dissociation of H_2O on Pt_{ML}/Mo_2TiC_2.

Notes: In alkaline solution(media), Volmer $H_2O + e^- + * \rightarrow *H + OH^-$, Heyrovsky $H_2O + e^- + * H \rightarrow * + H_2 + OH^-$. The barrier of H_2O dissociation is 0.92 eV. Therefore, it is difficult to occur HER in alkaline environment.

Table S1. Comparison E_{form} between different position of Pt monolayer on the Mo_2TiC_2 in a 2×2 supercell.

Possible position	**hcp**	**top**	**fcc**
$\boldsymbol{E_{form}}$**/eV**	-12.58	-10.02	-11.58
$\boldsymbol{E_{form}}$**/(eV/Å^2)**	-0.42	-0.34	-0.39

Table S2. Comparison work function of different structure.

	Work function Φ/eV
Pt_{ML}/Mo_2TiC_2	4.91
Mo_2TiC_2	4.65
Pt(111)	5.68
Metal Pt	5.65

Table S3. Adsorption energy (E_{ads}), average adsorption energy ($E_{ads(avg)}$) and stepwise adsorption energy ($E_{ads(step)}$) of hydrogen under different coverages on Pt_{ML}/Mo_2TiC_2.

Pt_{ML}/Mo_2TiC_2	E_{ads}/eV	$E_{ads(avg)}$/eV	$E_{ads(step)}$/eV
***H (0.25 ML)**	-0.30	-0.30	\
***2H (0.50 ML)**	-0.57	-0.29	-0.27
***3H (0.75 ML)**	-0.85	-0.28	-0.28
***4H (1 ML)**	-1.15	-0.29	-0.30
***5H (1.25 ML)**	-0.92	-0.18	0.23

Notes: From 0.25 ML to 1 ML, the average adsorption energy difference is within 0.02 eV, indicating that the surface adsorption is little affected by the coverage. Additionally, we show that atop H*, beyond a monolayer of hollow H* (1.25 ML), is unlikely to play a role in the HER mechanism due to its very positive adsorption energies ($E_{ads(step)}$ = 0.23 eV, $\Delta G_{ads(step)}$ = 0.48 eV).

Table S4. Adsorption energy of hydrogen on Pt(111) surface applying different functionals. The test slab model of Pt(111) was used 2×2 supercell with four atomic layer and the bottom two layer was fixed during optimization.

ΔG(*H)/eV	Pt(111)
PBE level	-0.25
PBE-D3 level	-0.34
RPBE level	-0.09
RPBE-D3 level	-0.21

Notes: The PAW pseudopotential and GGA-PBE exchange-correlation functional was used. And the Grimme' D3 correction for vdW dispersion was also considered in this work. Specially, for Pt(111), the adsorption energy of H has also tested using functional and found the value of -0.09 eV using RPBE functional, which was consistent with literature[14].

References:

1. G. Kresse and J. Furthmüller, *Comp. Mater. Sci.*, 1996, **6**, 15-50.
2. G. Kresse and J. Furthmuller, *Phys. Rev. B*, 1996, **54**, 11169-11186.
3. P. E. Blochl, *Phys. Rev. B*, 1994, **50**, 17953-17979.
4. A. D. Becke, *J. Chem. Phys.*, 2014, **140**, 9982-9985.
5. S. Grimme, J. Antony, S. Ehrlich and H. Krieg, *J. Chem. Phys.*, 2010, **132**, 154104.
6. H. J. Monkhorst and J. D. Pack, *Phys. Rev. B*, 1976, **13**, 5188-5192.
7. G. J. Martyna, M. L. Klein and M. Tuckerman, *J. Chem. Phys.*, 1992, **97**, 2635-2643.
8. G. Bussi, D. Donadio and M. Parrinello, *J. Chem. Phys.*, 2007, **97**, 014101.
9. W. Tang, E. Sanville and G. Henkelman, *J. Phys-Condens. Mat*, 2009, **21**, 084204.
10. V. L. Deringer, A. L. Tchougréeff and R. Dronskowski, *J. Phys. Chem. A*, 2011, **115**, 5461-5466.
11. S. Maintz, V. L. Deringer, A. L. Tchougreeff and R. Dronskowski, *J. Comput. Chem.*, 2016, **37**, 1030-1035.
12. G. Henkelman, B. P. Uberuaga and H. Jónsson, *J. Chem. Phys.*, 2000, **113**, 9901-9904.
13. J. K. Nørskov, J. Rossmeisl, A. Logadottir, L. Lindqvist, J. R. Kitchin, T. Bligaard and H. Jonsson, *J. Phys. Chem. B*, 2004, **108**, 17886-17892.
14. J. K. Nørskov, T. Bligaard, A. Logadottir, J. R. Kitchin, J. G. Chen, S. Pandelov and J. K. Nørskov, *J. Electrochem. Soc.*, 2005, **152**, J23-J26.
15. Y. C. Yao, X. K. Gu, D. S. He, Z. J. Li, W. Liu, Q. Xu, T. Yao, Y. Lin, H. J. Wang, C. M. Zhao, X. Q. Wang, P. Q. Yin, H. Li, X. Hong, S. Q. Wei, W. X. Li, Y. D. Li and Y. E. Wu, *J. Am. Chem. Soc.*, 2019, **141**, 19964-19968.
16. H. A. Hansen, J. Rossmeisl and J. K. Nørskov, *Phys. Chem. Chem. Phys.*, 2008, **10**, 3722-3730.
17. X. Huang, J. Wang, H. Bing Tao, H. Tian, Z. Zhang and H. Xu, *J. Catal.*, 2020, **389**, 461-467.
18. O. Vinogradova, D. Krishnamurthy, V. Pande and V. Viswanathan, *Langmuir*, 2018, **34**, 12259-12269.
19. Y.-W. Cheng, J.-H. Dai, Y.-M. Zhang and Y. Song, *J. Phys. Chem. C*, 2018, **122**, 28113-28122.
20. J. Liu, C. Q. Sun and W. Zhu, *Electrochim. Acta*, 2018, **282**, 680-686.
21. X. Hu, S. Chen, L. Chen, Y. Tian, S. Yao, Z. Lu, X. Zhang and Z. Zhou, *J. Am. Chem. Soc.*, 2022, **144**, 18144-18152.
22. Z. Duan and G. Henkelman, *ACS Catal.*, 2019, **9**, 5567-5573.
23. Z. Duan and G. Henkelman, *Langmuir*, 2018, **34**, 15268-15275.
24. Z. Duan and G. Henkelman, *J. Phys. Chem. C*, 2020, **124**, 12016-12023.
25. J. S. Filhol and M. Neurock, *Angew. Chem. Int. Edit.*, 2006, **45**, 402-406.
26. Z. Duan and G. Henkelman, *ACS Catal.*, 2020, **10**, 12148-12155.
27. C. D. Taylor, S. A. Wasileski, J.-S. Filhol and M. Neurock, *Phys. Rev. B*, 2006, **73**, 165402.
28. K. Mathew, R. Sundararaman, K. Letchworth-Weaver, T. A. Arias and R. G. Hennig, *J. Chem. Phys.*, 2014, **140**, 084106.